

Precision measurements of timing characteristics of the 8" ETL9351 series photomultiplier

19th November 2016

O.Ju.Smirnov¹, P.Lombardi², G.Ranucci²

Abstract

The results of the test measurements of the characteristics of 2200 PMT for the Borexino experiment provide the most complete information for the evaluation of the ETL9351 timing characteristics with a high precision. The unique timing characteristics of the apparatus used and the large statistics accumulated during the tests of the PMTs to be used in the future Borexino experiment, allow to resolve a fine structure of the PMT timing response.

A method to obtain the probability density function of the single photoelectron counting from the experimental data is proposed and applied to derive the PMT average characteristics. For the first time, an analytical model of the single photoelectron PMT time response is proposed, describing all the features of the single photoelectron time arrival. The origin of the small amplitude pulses is explained.

¹Corresponding author: Joint Institutur for Nuclear Research, 141980 Dubna, Russia. E-mail: osmirnov@jinr.ru;smirnov@lngs.infn.it

²Dipartimento di Fisica Università and I.N.F.N., Milano, Via Celoria, 16 I-20133 Milano, Italy

1 Introduction

Photomultipliers with a large area spherical photocathode are being widely used in many liquid scintillator and water cherenkov rare events detectors. All recently developed solar neutrino detectors, such as SNO [1], KamiokaNDE [2], KamLAND [3], Borexino [4] and its Counting Test Facility [5], are based on the scintillation photons counting techniques. The interaction point in these detectors is reconstructed using timing information from a large number of PMTs. Depending on the precision of reconstruction and the total number of PMTs the precision of single photoelectron detection at the level of 1 ns is demanded. The Monte Carlo simulation of the Borexino detector showed that the mean number of photoelectrons (p.e.) registered by one PMT in a scintillation event will be in the region $0.02 - 2.0$ for an event with energy of 250-800 keV. Hence the PMTs should demonstrate a good single electron performance. After preliminary tests, the ETL 9351 with a large area photocathode (8") has been chosen [7]. The PMT of this model has 12 dynodes with a total gain of $k = 10^7$. The transit time spread of the single p.e. response is $1 - 1.5$ ns. The PMT has a good energy resolution characterized by the manufacturer by the peak-to-valley ratio. The manufacturer (Electron Tubes Limited, ETL) guarantees a peak-to-valley ratio of 1.5. The results of the preliminary tests with 50 PMTs have been reported in [6].

2 PMT test facility at LNGS

In the Borexino programme the special PMT test facility was prepared at LNGS. The test facility is placed in two adjacent rooms. In one room the electronics is mounted, and the other is a dark room with 4 tables designed to hold up to 64 PMTs. The dark room is equipped with an Earth's magnetic field compensation system using rectangular coils with an electric current ([11]). The non-uniformity of the compensated field in the plane of the tables is no more than 10%. The tables are separated from each other by black shrouds, which screen any light reflected from the PMTs photocathode.

The simplified scheme of one channel of electronics (out of the total 32) of the test facility is presented in Fig.1. The system uses the modular CAMAC standard electronics and is connected to a personal computer by the CAEN C111 interface. The PMT characteristics are normally measured during a 5 hour run.

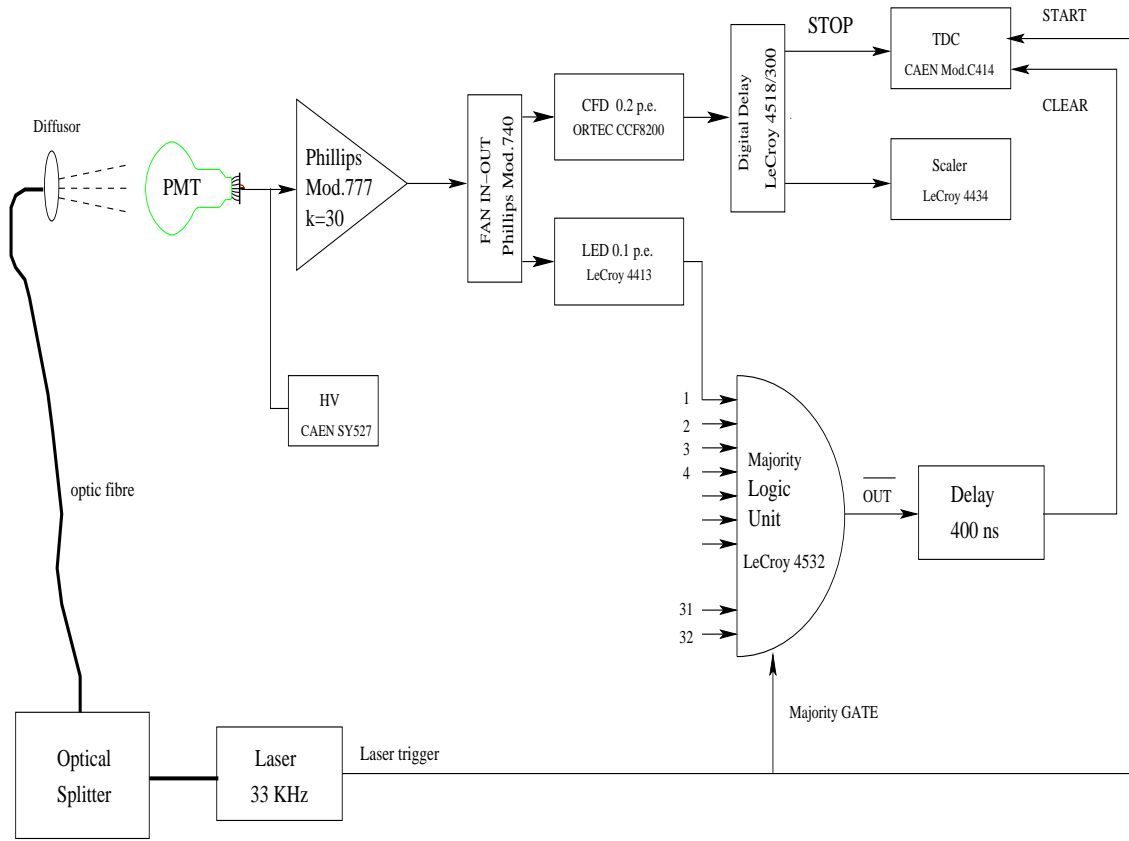


Figure 1: The simplified scheme of the one channel of the electronics.

The PMTs are illuminated by low intensity light pulses from a laser. A picosecond Hamamatsu pulse laser was used in the tests. The model used has a peak power of 0.39 mW , the pulse width is 27.3 ps , and the laser wavelength is 415 nm , which is close to the maximum sensitivity of the ETL 9351 photocathode. The light pulse from the laser is delivered by 6 meter long optical fibers into the dark-room. Each of the 4 fibers is supplied with a diffuser in order to provide a more uniform illumination of the tables.

The TDC, CAEN mod.C414, “start” signals are generated using the laser internal trigger, which has negligible time jitter ($< 100\text{ ps}$) with respect to the light pulse. The “stop” signal for the TDC is formed by the constant fraction discriminator (CFD, ORTEC mod.CCF8200) with the threshold set at the 0.2 p.e. level. The full scale of TDC was set to 200 ns with 2048 channels resolution. Because of the memory restrictions of the software, only the part of the full range was used, namely 100 ns in the region $[-30\text{ ns};+70\text{ ns}]$ around the main peak in the PMT transit time.

The 32-input majority logic unit, LeCroy mod.4532, is able to memorize the

pattern of the hit channels. This information significantly increases the data processing rate. The reading of the electronics is activated when the majority LAM signal is on (a LAM is produced if one of the signals on the input is inside the external GATE on the majority logic unit). Otherwise, a hardware clear is forced using the majority \overline{OUT} signal. Every pulse of the laser is followed by an internal trigger. The trigger is used as the majority external gate.

A high precision calibration of each electronics channel had been performed before the measurements. Here calibration means the precise knowledge of the response to a signal corresponding to 1 p.e.¹ on the system input. The PMT in this measurement was substituted by a precision charge generator LeCroy mod. 1976.

The gain of each PMT electron multiplier was set to a value of $2 \cdot 10^7$, before the tests with a help of automated gain adjustment system, described in [12].

3 Results of the 2000 PMT testing

The main timing characteristics defined during the acceptance tests were:

- t_0 and σ_t the position and the rms of the gaussian fitting the main peak in the transit time distribution. The fit had a an additional constant corresponding to the dark noise level;
- rms is estimated for all transit time histogram (up to 90 ns);
- p_{late} late pulsing in percent, estimated as the ratio of the events in the $[t_0 + 3 \cdot \sigma_t; 100]$ ns range to the total number of the events;
- p_{prep} prepulsing in percent, estimated as the ratio of the events in the $[0; t_0 - 3 \cdot \sigma_t]$ ns range to the total number of the events.

The results of measurements showed no essential problems with the transit time spread of the PMTs, with PMTs rejected mainly or because of the high dark rate or because of the bad amplitude response of the PMT. As a rule a PMT with a good single photoelectron charge response has also a good timing response.

The results of the measurements are presented in Table 1. For future use we put also in this table the parameter p_U , which is the fraction of the underamplified signals in the amplitude spectrum of the single photoelectron response. The model

¹multiplied by a factor of 10^7 by the electron multiplier and giving 1.6 pC charge

used to extract the value for p_U from the single p.e. charge response is described in [8]. The underamplified signals can be described well with an exponential with a negative slope $A = -0.17$ p.e., the value of A is presented in Table 1 too. The measurements with a threshold (Th) set to 0.16 p.e. cuts 61% of the underamplified signals, leaving 6.4% of the total 16.5%.

The distribution of the t_0 , σ_t and rms parameters is a normal distribution with a sigma coinciding with the rms of distribution. The distributions for p_{late} and p_{prep} have longer non-gaussian tails. All these results have been written in a database, which can be used for the detector modeling.

Table 1: The results of test.

parameter	t_0 ns	σ_t ns	rms ns	p_{late} %	p_{prep} %	p_U	A p.e.	Th p.e.
mean	32.59	1.18	8.14	7.27	0.69	0.165	-0.17	0.16
rms	3.85	0.11	0.54	1.0	0.30	0.05	0.068	0.04

An important characteristic of the PMT is the dependence of the peak of the transit time t_0 on the applied voltage, see Fig.2. The shift of the t_0 position due to a change in the voltage applied is 0.02 ns/V. This value can be used in order to equalize the time arrival of photoelectrons after each adjustment of the high voltage.

4 The averaged transit time shape

The straightforward use of the database, with a set of parameters for each PMT, for the detector's modeling will unnecessary slow down the calculations, because of the huge number of PMTs (2200) used in the experiment. The calculation speed can be improved using average characteristics of the PMTs instead of the individual ones. Because every PMT operates at its own voltage, and the lighting conditions depends on the position on the test tables, the procedure of averaging should be preceded by the equalizing the difference in the conditions. Fortunately, the statistics of the first photoelectron counting provides this possibility.

4.1 Statistics of the first photoelectron time arrival

With any experimental conditions, the PMT does not register single photoelectron, and so the single photoelectron response should be extracted from a PMT

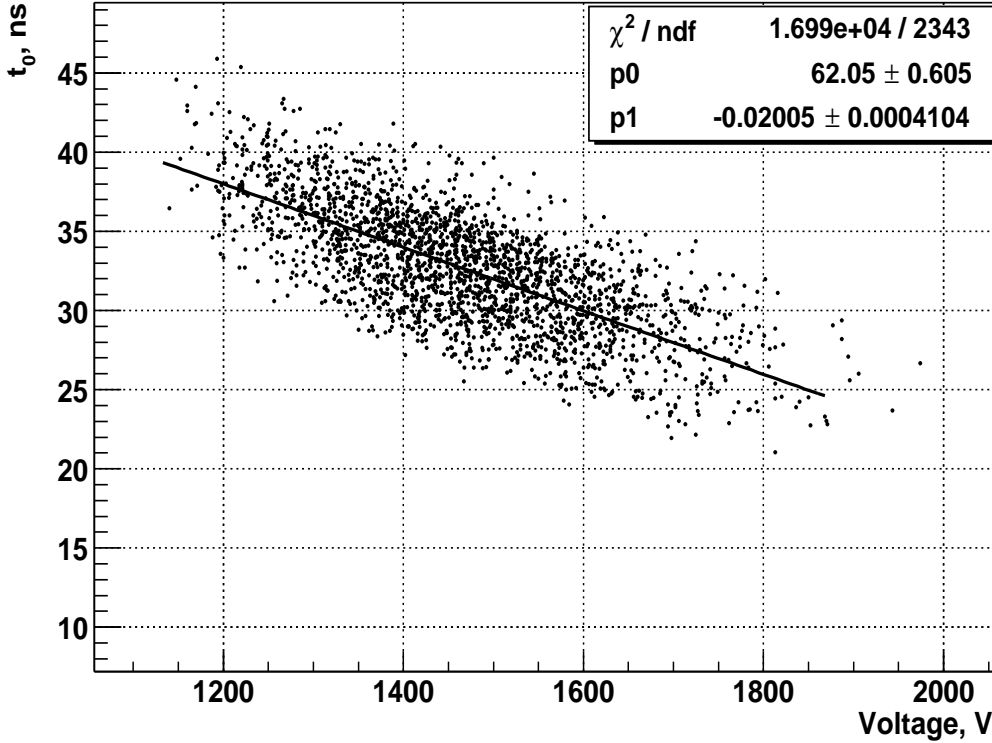


Figure 2: The dependence of the transit time peak on the applied voltage.

response [9, 10]. The basic assumption in the following considerations is a Poisson distribution for the amount of the registered photoelectrons.

If the probability density function (p.d.f.) of a single p.e. registering at time t is $\rho_1(t)$, then the probability to observe the first p.e. out of precisely n photoelectrons at time t is

$$\rho_n(t) = n \cdot \rho_1(t) \cdot (1 - F_1(t))^{n-1} \quad (1)$$

where $F_1(t) = \int_{-\infty}^t \rho_1(t') dt'$ is probability to observe a single p.e. before time t .

The equivalence of the photoelectrons gives the factor n , and $(1 - F(t))^{n-1}$ is the probability of not observing any of the remaining $(n - 1)$ p.e. before time t .

If the number of photoelectrons is not fixed, but distributed in accordance to a Poisson law with a mean μ p.e. per pulse, then the probability of the arrival of the first signal at the PMT can be calculated by averaging (1) over the Poisson distribution $P(n) = \frac{\mu^n}{n!} e^{-\mu}$:

$$\rho(\mu, t) = \mu \rho_1 e^{-\mu F_1(t)}. \quad (2)$$

The p.d.f. in (2) is normalized by the total probability of the presence of a non-zero signal for a Poissonian distribution $P(n > 0) = 1 - e^{-\mu}$:

$$\int_{-\infty}^{+\infty} \rho(\mu, t) dt = 1 - e^{-\mu},$$

which can be easily checked out noting that $\rho_1(t)dt = dF(t)$.

The full probability to register a signal in the interval $[-\infty, t]$ is then:

$$F(\mu, t) \equiv \int_{-\infty}^t \rho(\mu, t') dt' = 1 - e^{-\mu F_1(t)}. \quad (3)$$

From (2) and (3) follows a simple relation:

$$\rho_1(t) = \frac{1}{\mu} \frac{\rho(\mu, t)}{1 - F(\mu, t)}. \quad (4)$$

which allows to calculate the $\rho_1(t)$ function using experimental data.

If experimental data are presented in the form of a histogram $N_{Exp}(i)$, then the probability density function of the single photoelectron can be calculated in accordance with (4):

$$N_1(i) = \frac{1}{\mu} \frac{N_{Exp}(i)}{1 - s(i)}, \quad (5)$$

where

$$s(i) \equiv \frac{1}{N_{Triggers}} \sum_{k=1}^{k=i} N_{Exp}(k) \quad (6)$$

is the running sum of the histograms of the experimental data $N_{Exp}(i)$ normalized by the number of the system starts $N_{Triggers}$. Naturally, when $N_{Triggers}$ is large enough, one can expect $s(\infty) = 1 - e^{-\mu}$.

For completeness, let us give the equation for the estimation of the errors in $N_1(i)$:

$$\sigma_1(i) = \frac{1}{\mu} \frac{\sigma(i)}{1 - s(i)}.$$

The equation (4) is especially useful when calculating the function $\rho_1(t)$ from the experimental data with $\mu \simeq 1$, where the shape of $\rho(t)$ is significantly different

from the shape of $\rho_1(t)$, and the approximation $\rho(t) \simeq \mu\rho(t)$ can not be considered satisfactory. In our measurements the $\mu \simeq 0.05$ and the correction applied is of the same order at the distribution tail (at small μ the approximation $F(t_{Max}) \simeq \mu$ is valid).

4.2 Correcting for the random coincidence with a dark noise

The laser system has been tuned to provide mean counting rate of the PMTs $\mu \simeq 0.05$ p.e.; this condition ensures a mostly single p.e. regime for the PMT (with the relative probability of the signal originating from 2 p.e. and more $r = \frac{P(n>1)}{P(n>0)} = \frac{1-e^{-\mu}-\mu e^{-\mu}}{1-e^{-\mu}} \simeq \frac{\mu}{2}$, i.e. 2.5 %). With such a small amount of light in a pulse, the PMT response could be affected by the dark noise of the PMT, which is of the order of some kHz. The probability of the random coincidences due to the dark noise f_{dark} in the time window τ can be expressed by

$$f_{rndm} = f_{dark} \cdot \tau,$$

and the total amount of dark noise counts in each bin of the histogram (of the total N_{bins}) is

$$N_{dark}(i) = N_{Triggers} \frac{f_{rndm}}{N_{bins}}.$$

In order to take correctly into account the random noise in the system one should substitute $N_{exp}(i)$ by $N_{exp}(i)-N_{dark}(i)$ in equations (5) and (6).

The dark noise in the system is measured independently with high precision using scalers.

4.3 The procedure used to obtain the mean characteristics of the PMT

1. Using the measured value of the dark rate the contribution N_{dark} of the random coincidences at one bin was calculated.
2. Using equations (5) and (6) with $N_{exp}(i)$ substituted by $N_{exp}(i)-N_{dark}(i)$ the

$N_1(i)$ function was calculated and normalized:

$$n_1 = \frac{N_1(i)}{\sum_{i=1}^{N_{bins}} N_1(i)}. \quad (7)$$

As follows from (7), the knowledge of the mean number of the registered photoelectrons is not necessary for the calculation of the normalized probability.

3. The peak in the distribution n_1 is found and the histogram is shifted in order to put its maximum at the position corresponding to $t = 0$.
4. All the histograms are summed together and normalized to 1 once more. The obtained histogram contains the mean characteristics of the sample of the PMTs used with a peak (not mean time of the arrival) at the position $t = 0$.

The resulting histogram is presented in Fig.3. This is the PMT transit time p.d.f. averaged over a 2000 PMT sample.

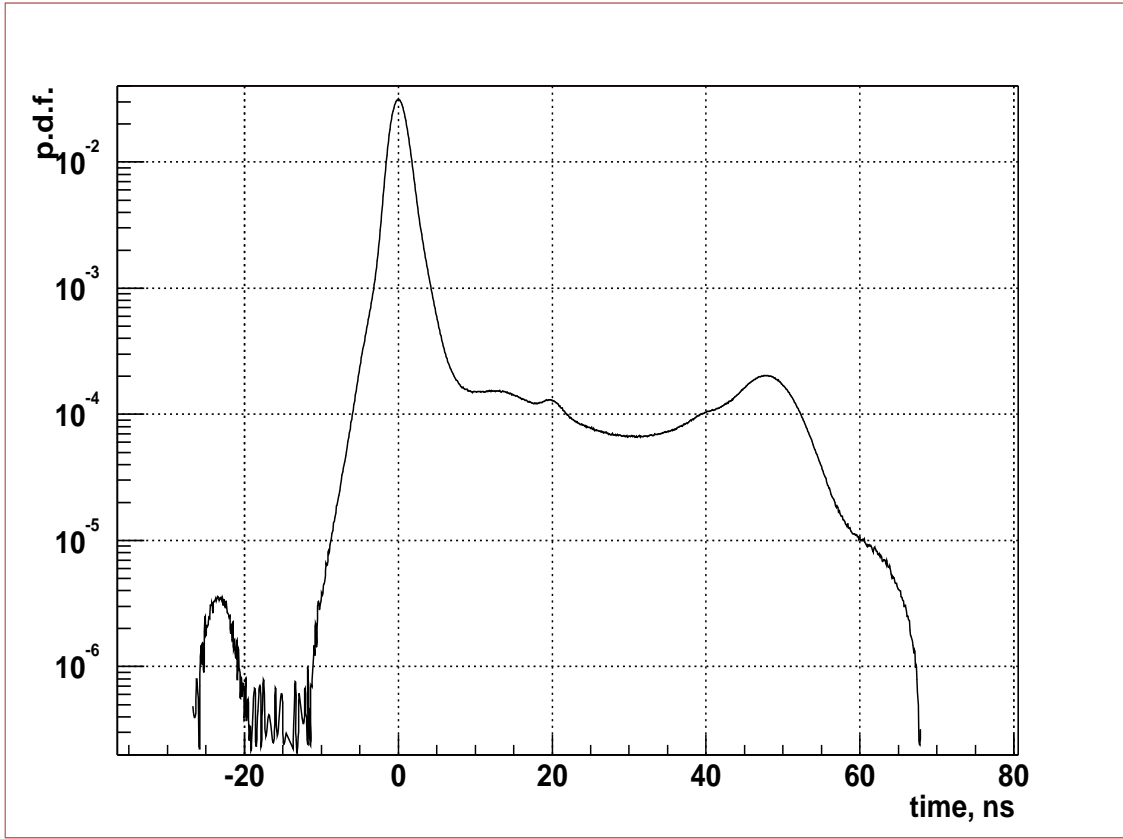


Figure 3: The averaged timing characteristics of the ETL9351 PMT.

5 The structure of the photomultiplier transit time

The following features of the transit time curve can be clearly seen in Fig.3: 1)almost gaussian peak at the position $t = 0$ ns; 2)a very weak peak at $t = -24$ ns; 3)a weak peak at $t = 48$ ns; 4)the continuous distribution of the signals arriving between the main peak and the peak at $t = 48$ ns; 5)another very weak peak at $t = 20$ ns. All these features, together with others appearing with closer investigation of the curve, will be explained in the current section.

5.1 Main peak

The fine structure of the main peak can be seen in Fig.4. The main peak has almost gaussian shape, but at the regions $t > 2$ ns and $t < -2$ ns the deviation from the gaussian distribution is significant. Early pulses can arrive due to the elastic scattering of the photoelectron on the first dynode without multiplication, in such a way arriving at the next stage of the electron multiplier earlier than secondaries do. The same process can occur on the second dynode, third etc. The energy of the electron arriving at the first dynode is defined by the potential difference between the photocathode and the first dynode U_{D1} . The U_{D1} voltage is constant in the divider scheme used, which is provided by three Zenner diodes of 200 V each. The energy gained by the elastically scattered electron at the second stage is small in comparison to the initial 600 eV, thus the velocity of the electron in the sequence of the elastic scatterings can be considered constant in first approximation, as well as the transit time between the first dynodes. The arriving of the early signals can be modeled by a set of the equidistant gaussians with the same spread and geometrically decreasing strength:

$$f_e(t) = \frac{1}{p + p^2 + \dots + p^N} \sum_{n=1}^N \frac{p^n}{\sqrt{2\pi}\sigma_e} e^{-\frac{1}{2}(\frac{t+n\delta_t}{\sigma_e})^2}. \quad (8)$$

The pulses just after the main peak are due to the inelastic scattering on the first dynode.

Let us introduce a set of variables, describing the relative probabilities of the considered processes: p_g is the relative probability of the signals under the gaussian part of the peak; the early pulses arrive with a relative probability p_e and the late pulses have a relative probability p_l .

We will describe the late pulses using a function:

$$f_l(t) = \frac{\sigma_l^2 - (t - t_l) \cdot \tau}{2\tau^2} (1 + \operatorname{erf}\left(\frac{(t - t_l) \cdot \tau - \sigma_l^2}{\sqrt{2} \cdot \tau \cdot \sigma_l}\right)) \quad (9)$$

which is a convolution of an exponential with a slope $\frac{1}{\tau}$, and a gaussian with sigma σ_l .

The main peak fits well with the following function:

$$M(t) = p_g \cdot f_g(t - t_0) + p_e \cdot f_e(t - t_0) + p_l \cdot f_l(t - t_0) \quad (10)$$

The results of the fit can be seen in Fig.4 and Fig.5. The parameters of the best fit are presented in Table2. The model of the main peak describes 94 % of all pulses.

Table 2: The parameters of the best fit.

p_g	p_e	p_l	t_0	σ	p	δ_e	σ_e	τ	t_l
0.83	0.023	0.085	0.02	1.04	0.06	3.3	1.29	0.92	1.80

The time of flight between the dynodes $\delta_t = 2.76$ ns corresponds to the difference in the time of flight of the fast electron between the dynodes and the drift time of the secondary electrons.

The amplitude of the early pulses was not measured in our tests, but some can be deduced from the model of the early pulsing. The coefficient of the multiplication at energies $E_e > 600$ eV is almost independent on energy. Thus, a photoelectron missing the first stage of multiplication (with mean gain g_1) and multiplied at the second stage with a gain g_1 instead of g_2 will produce at the anode a signal with a mean amplitude reduced by the factor $f_1 = \frac{1}{g_2}$, which is normally in the range 0.2 – 0.3. The reduction factor f_2 for a photoelectron missing two first stages of multiplication will be $f_2 = \frac{1}{g_2 \cdot g_3}$, etc. As one can see from Table.2 the geometrical progression factor is much lower, $p = 0.06$ because of the threshold effect. In order to estimate the part of the signals over the threshold we note that the underamplified signals have an exponential distribution. The decrease in amplitude of the signal corresponds to the increase of the slope of the exponential distribution. If the threshold is fixed, then the part of the signals over the threshold is $p = (e^{-\frac{q_{th}}{A}})^{g_2}$ for the signals missing the first stage of amplification. $A = 0.17$, the mean threshold is $q_{th} = 0.16$, and $g_2 \simeq 3$, hence $p \simeq e^{-3} \simeq 0.05$, in agreement with the fit value. The same rule is valid for the electrons missing two and more stages of amplification.

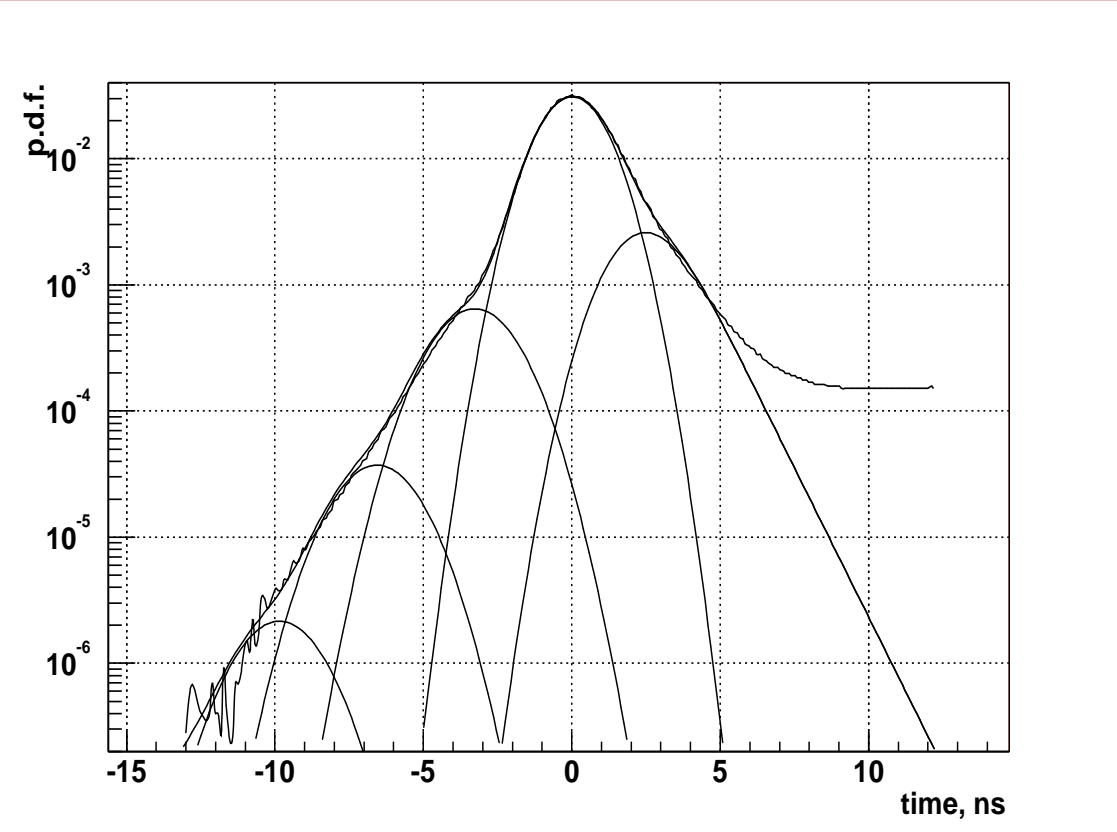


Figure 4: Main peak region

5.2 Prepulses

In the transit time histogram can be clearly seen a small peak at about -24ns. These are so called prepulses, corresponding to the direct photoproduction of the electron on the first dynode. The amplitude of these pulses is factor g_1 (amplification of the first dynode) less then the amplitude of the main peak. Because a typical value is $g_1 \simeq 10$, these pulses are strongly suppressed by the CFD threshold set at the 0.2 p.e. level. The shape of the peak is well approximated by a gaussian (see Fig.6) with a parameters given in Table 3.

Table 3: The parameters of the prepulses peak.

p_{pp}	t_{pp}	σ_{pp}
$1.22 \cdot 10^{-4}$	-23.18	1.39

The difference $dt = 23.2$ ns between the position of the main peak t_0 , and the position of the prepulses peak t_{pp} corresponds to the drift time of the electron from

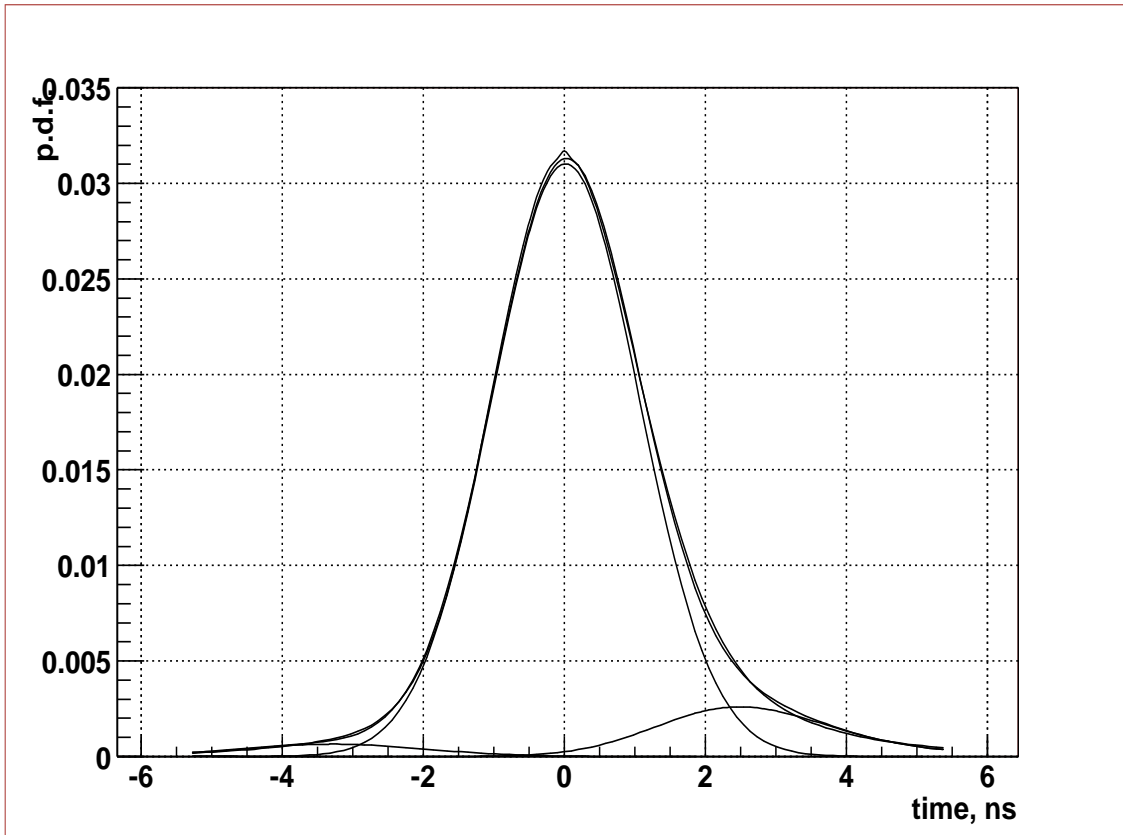


Figure 5: Main peak region on the linear scale.

the photocathode to the first dynode t_d with the time of flight of photon to the first dynode t_{tof} subtracted: $dt = t_0 - t_{pp} = t_d - t_{tof}$. The time of flight can be calculated from the known distance between the photocathode and the first dynode, which is 123 mm (radius of the spherical photocathode is 110 mm, the focusing grid is situated at the center of the sphere, the distance between the focusing grid and the first dynode is 13 mm). Hence the time of flight of photon inside the PMT is $t_{tof} = 0.41$ ns, and the drift time $t_d = dt + t_{tof} = 23.61$ ns. The drift time is the same for all the PMTs tested, because the potentials difference between the photocathode and the first dynode is stabilized.

In setups with a large number of PMT in use, the presence of prepulses is a potential source of the early triggers in the system.

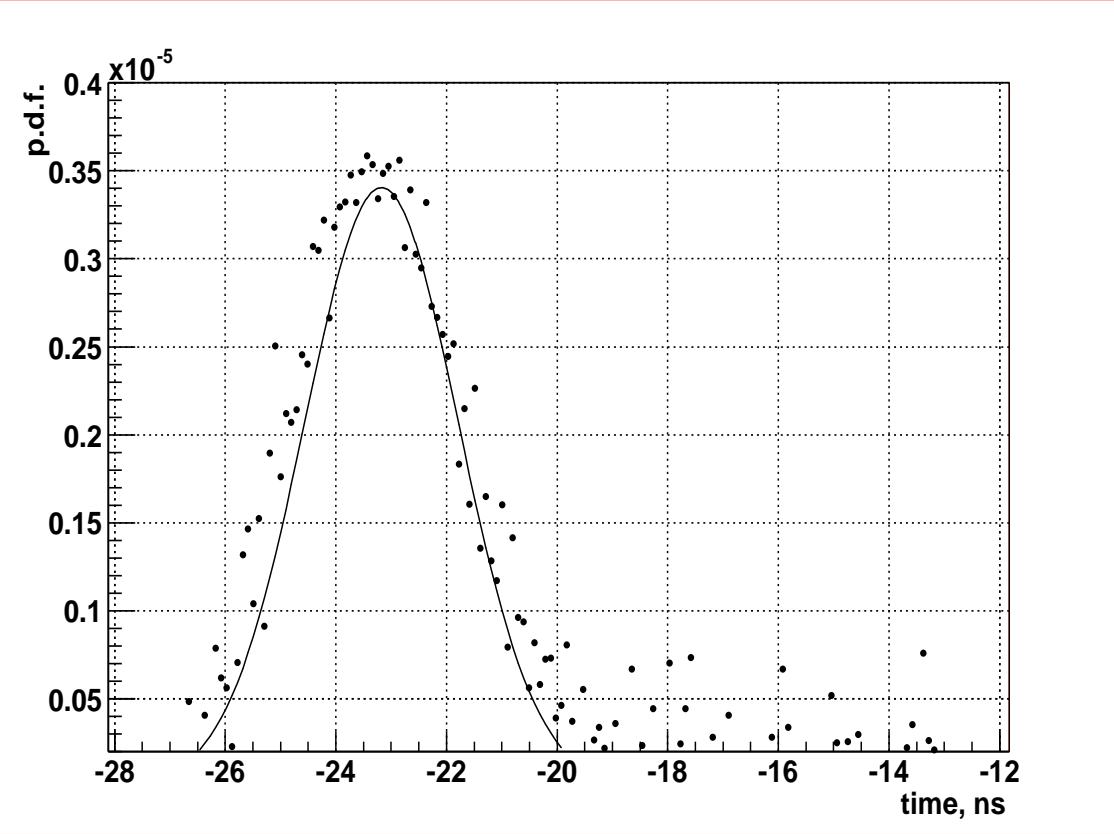


Figure 6: Prepulses

5.3 Late pulses

Pulses arriving after the main pulse, in the time range up to 100 ns, are called late pulses. The structure of the late pulses spectrum can be seen in Fig.7. We are not considering here pulses arriving in the microseconds interval, which are caused by the ion-feedback. In literature these pulses are called afterpulses.

The shape of the late pulses is modeled well with a sum of 3 functions of the type given in equation (9).

The parameters of the best fit are presented in Table 4. It should be noted that the function $M(t)$ describing the main peak has been fixed during the fit of the late pulses shape.

The peak with probability $p_r = 5.8 \cdot 10^{-4}$ at $t = 20.23$ ns is caused by the light feedback on the laser optical splitter system. The light guide of about 1.5 m delivers photons from the laser head to the optical splitter. On the output of the light guide there is a lens focusing light on the bunch of light guides, which in turn

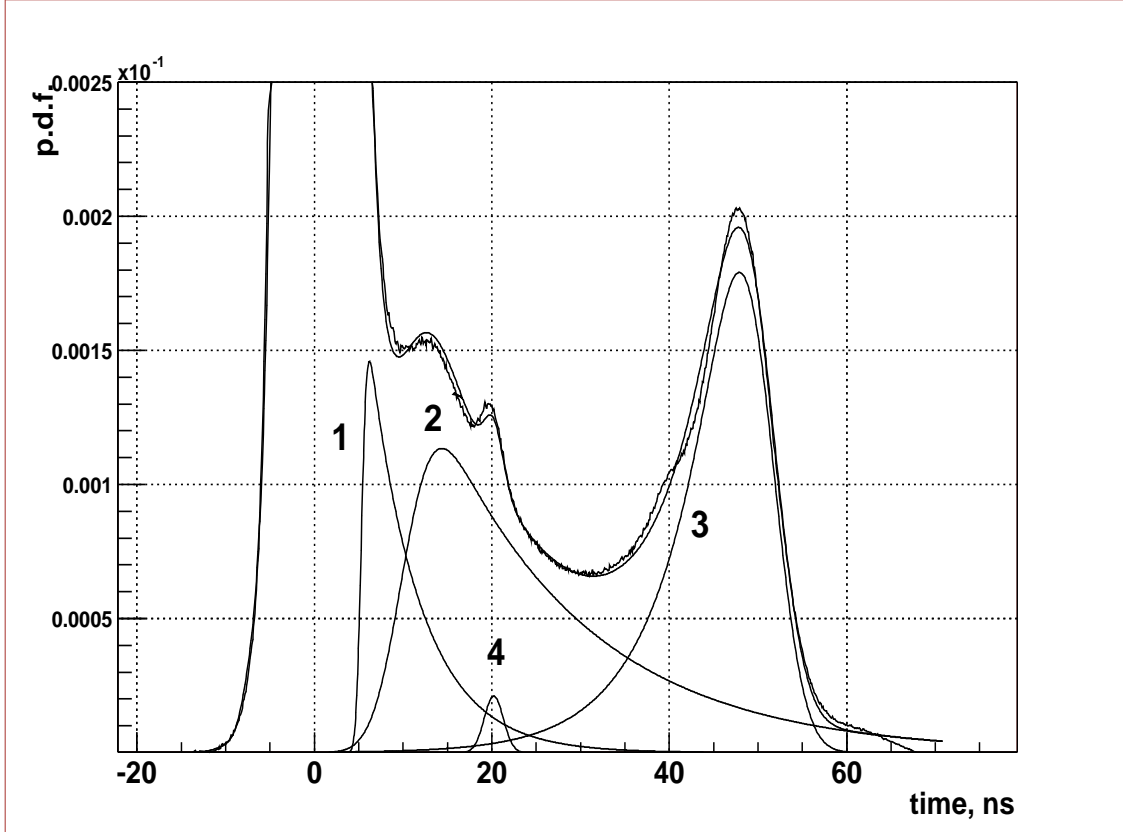


Figure 7: Late pulses. Lines 1 and 2 corresponds to inelastically scattered photoelectrons, curve 3 describes elastically scattered photoelectrons. Gaussian shape 4 describes light reflections in the light splitting system.

Table 4: Late pulses fit parameters

component	p_1	t_1	σ_1	τ_1
1	0.011	4.92	1.40	5.69
component	p_2	t_2	σ_2	τ_2
2	0.027	10.1	2.73	16.8
elastic component	p_{el}	t_{el}	σ_{el}	τ_{el}
	0.024	51.0	2.89	-6.52

are delivering light to the dark room. In order to provide a single photoelectron regime, a reflective attenuation filter is placed between the lens and fibers input. The filter reflects part of the light, which after traveling back and forth between the filter and the laser head can be fed back to the system². The spread of the peak

²The light splitting system has been manufactured by independent professional and has been used as is. The reflection peak can be seen only with a high statistics data, and was noted only after the final data processing. The hardware problem could be easily solved rotating filter by a

$\sigma = 1.07$ ns coincides with a main peak spread. This peak was extracted from the final shape.

The remaining late pulses shape is described by three functions given by equation (9) type, two with negative and one with a positive slope (signs in eq. (9) are inverted). The position of the last peak helps in clarifying its origin. The difference between the position of the last peak and the main peak is $\Delta t = 47.6$ ns³, and it is in perfect coincidence with a double drift time obtained in the previous subsection: $2t_d = 47.2$ ns. The double drift time can be explained by electrons which elastically scatter on the first dynode electrons, then go away from the dynode, slows down and stops near the photocathode, and then go back to the first dynode to produce a signal. The amplitude of this pulses should be the same as that of the main peak pulses, which is confirmed in [13] by measuring the transit time of the PMT with a higher threshold. The total probability to observe elastically scattered photoelectron is $p_{el} = 0.024$.

Two remaining contributes with a negative slope corresponds to an inelastic scattering of the photoelectron on the first dynode, without any secondaries produced. In this case, part of initial energy of the incident electron is dissipated as heat in the material of the dynode, and the drift time of the electron in this case depends on the remaining part of the energy, and, naturally, is less than in the case of elastic scattering. In the extreme case all the energy is dissipated, and, without any delay, the electron is transferred to the next stage of amplification, producing on average a signal with an amplitude of factor g_1 smaller than a normal signal. In the intermediate case, the scattered electron is delayed by the time in the range $0 - 2t_d$, and after returning back to the first dynode produces a signal with lower amplitude in comparison to the amplitudes of the main peak signals. The smaller is the delay the smaller is the amplitude of the signal.

The total amount of the inelastically scattered photoelectrons can be defined summing these two contributes to the late pulses. The summing gives a value $p_{in} = 0.038$, i.e. almost 4% of all registered signals are the signals of small amplitudes due to inelastically scattered photoelectrons. This value is less than a value of 6.4% obtained in section 3 using the values of p_U , A and the TDC threshold from Table small angle.

³We are using here results of the separate fit of the position of the last peak with a gaussian. The parameter t_{el} from the Table 4 can't be used in this estimation, because the model function (9) gives .. of the many individual contributions. For example the function of the form (9) can be used to fit the early pulses shape instead of (8) with a same result.

1. A contribution of 8.4% from the main peak fit..... This observations leads to a conclusion that the underamplified part of the signals is mainly due to the totally inelastic scattering on the first dynode with a minimal delay. The amplitude of the pulses arriving at $t > 5$ ns is bigger than a threshold set. In fact, when fitting the charge spectrum of the PMT with a sum of exponential and gaussian terms, the valley between them remains underfilled.

The proposed model fits well the observed distribution; nevertheless, the statistics are so high that some further features of the transit time of elastically scattered photoelectrons can be noted. At the increasing part of the elastic peak there is a small bump in the region of 41 ns (see Fig.8). The amount of this pulses is very small, but the bump is pronounced. These are the photoelectrons, elastically scattered from the focusing grid before the first dynode. These electrons can reach the photocathode, and after the elastic scattering on the photocathode, or possible multiplication on it it will arrive to the first dynode with an energy of the normally accelerated electrons. In the case of multiplication on the photocathode this results in a bigger amplitude signals. This can partially explain the non-gaussian tails observed in the charge distribution of the single photoelectron signals.

6 Discussions

The method proposed for the deconvolution of the PMT signal can be used as well to extract the time decay curve of the liquid scintillator, using the data obtained with the start-stop measurements with TDC.

No signals have been observed at the position corresponding to the single drift time of photoelectron t_d , that would have been present in the case of generation of luminiscent photons or gamma-rays on the first dynode by an incident photoelectron, without producing secondaries. The presense of the small peak, nearly at the same position due to the reflections in the light splitting system gives a possibility to estimate the sensitivity of our setup to this kind of process at the level of 10^{-5} (one should note, that the peak with a probability $5.8 \cdot 10^{-4}$ is clearly seen, and the position of the hypothetical peak is known).

The good knowledge of the PMT timing response can help the manufacturer in improving the PMT timing characteristics. From the point of view of the experimentor, a good knowledge of the PMT response is necessary for the proper modeling of the detector response, and in most practical cases one can simplify the

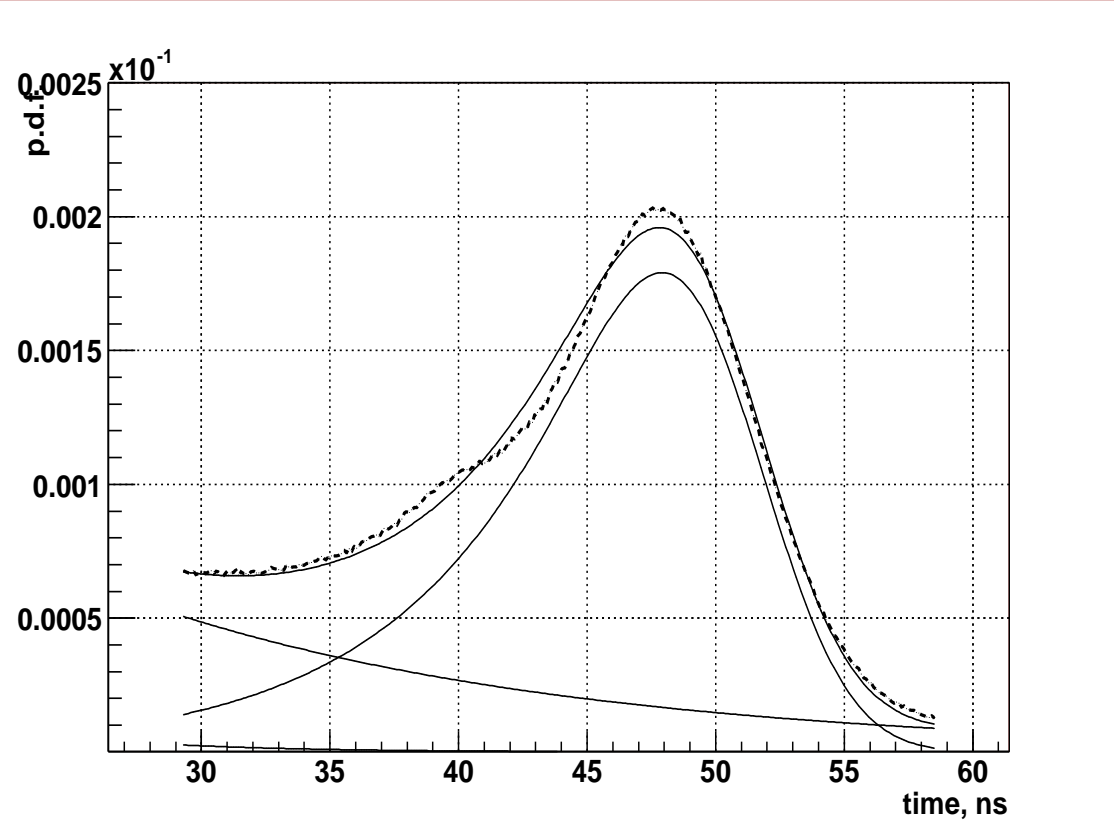


Figure 8: The bump on the transit time curve can be clearly seen at 41 ns.

model, keeping only the main contributions to the signal. In Fig.9 are shown PMT responses modeled with a $\rho_1(t)$ function and with a function $M(t)$ without the early pulses term. One can see that the function $M(t)$ fails to describe the PMT timing response, and the function $\rho_1(t)$ practically coincide with $\rho(\mu, t)$, reflecting the fact, that the PMT operates mainly in a single p.e. regime.

Another case is illustrated in Fig.10. The PMT is registering on average $\mu = 5$ p.e. The tail in the PMT transit time distribution is suppressed by more than one order of magnitude, and the $\rho_M(t)$ function gives a satisfactory description of the $t > 0$ ns part of the distribution. But this time, the early pulses should be taken into account in order to have a good model of the early coming pulses.

We can conclude, that the multiple p.e. signal can be modeled with a main peak part of the total distribution, given by equation (10). In the case of a single photoelectron counting the best result can be obtained using the $\rho_1(t)$ function.

The prepulses at $t = -24$ ns stays far away from the main peak, and with a proper treatment can be easily separated. The amplitude of these pulses is small,

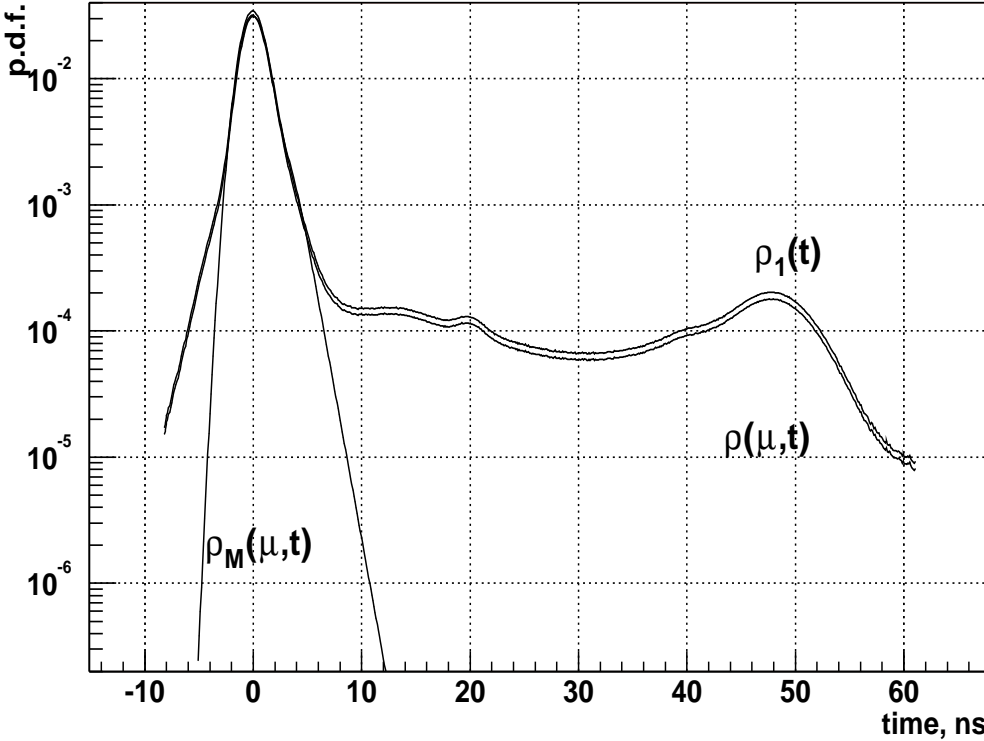


Figure 9: The modeled PMT response to the $\mu = 0.25$ p.e. light source $\rho(\mu, t)$, the single photoelectron response $\rho_1(t)$ and the model of the PMT response with only two terms of the main peak function (without early pulses), $\rho_M(\mu, t)$.

and they can be suppressed increasing the threshold, as it was demonstrated in [13]. In general, the relative probability of prepulses increases almost linearly with an increase of the mean number of the registered photoelectrons: $p_{pp} \simeq \mu \cdot p_{pp}^1$, where p_{pp}^1 is a relative probability of the early pulses in the single p.e. regime. At $\mu = 10$ p.e. it is still of the order of 10^{-3} .

7 Conclusions

The results of the test measurements of the characteristics of 2200 PMT for the Borexino experiment provide the most complete information for the evaluation of the ETL9351 timing characteristics with a high precision. The unique timing characteristics of the setup used and a huge statistics accumulated during the tests of the PMTs to be used in the future Borexino experiment, allow to resolve the fine

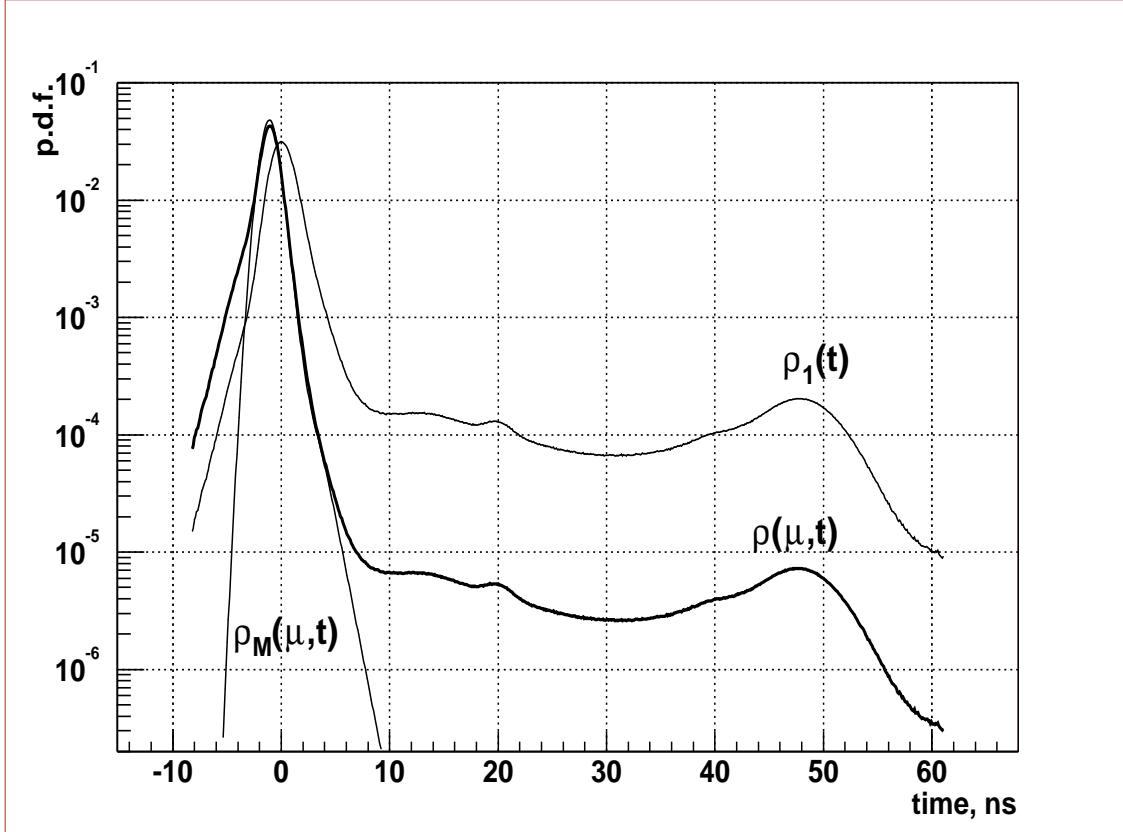


Figure 10: The modeled PMT response to the $\mu = 5$ p.e. light source, $\rho(\mu, t)$, the single photoelectron response $\rho_1(t)$ and the model of the PMT response with only two terms of the main peak function (without early pulses), $\rho_M(\mu, t)$.

structure of the PMT timing response.

A method to obtain the probability density function of the single photoelectron counting from the experimental data is proposed and applied to derive the PMT average characteristics. For the first time an analytical model of the single photoelectron time arrival in a PMT is proposed, describing all the features of the single photoelectron time arrival. The origin of the small amplitude pulses, as well as a non-gaussian tail in the amplitude response of PMT are explained.

8 Acknowledgements

Credits are given to the developers of the CERN ROOT program [14], that was used in the calculations and to create all the figures of the article. Special thanks to R.Ford for the careful reading of the manuscript.

References

- [1] SNO Collaboration, Boger J., et al, NIM A449(2000)172.
- [2] Kamiokande Collaboration, Hirata K.S., et al, Phys.Rev.Lett. 65(1990)1297.
Fukuda Y., et al, Phys.Rev.Lett. 77(1996)1683.
- [3] Suzuki A., Nucl.Phys. B 77(Proc.Suppl.)(1999)171-176.
- [4] G. Alimonti et al., BOREXINO Collaboration, Astroparticle Physics 16 (2002)
205-234.
- [5] Alimonti G. et al., Nucl. Instrum. and Methods. A 406 (1998) p.411-426.
- [6] G. Ranucci, D.Giugni, I.Manno et al., Nucl. Instrum. and Methods. A337
(1993) 211.
- [7] Photomultipliers and Accessories, Electron Tubes Ltd., p.56.
- [8] R. Dossi, A. Ianni, G. Ranucci, O. Ju. Smirnov. NIM A451 (2000) 623.
- [9] G. Ranucci, NIM A335 (1993) 121.
- [10] G. Ranucci et al., NIM A350 (1994) 338.
- [11] G.Bacchicocchi , A. Brigatti, R. Dossi, A. Ianni,..O. Smirnov. "The Earth's magnetic field compensation in the Borexino Phototubes facility." LNGS preprint
INFN/TC-97/35, 1997. Available at <http://lnsgs.infn.it/>.
- [12] O. Ju. Smirnov. Instruments and Experimental Techniques, Vol.45 No3 (2002)
363.
- [13] B.K.Lubsandorzhiev, P.G.Pokhil, R.V.Vasiljev, A.G.Wright. NIM A 442 (2000)
452.
- [14] <http://root.cern.ch/>